Propagation of resonant 0π pulses in rubidium

U. Kallmann, S. Brattke, and W. Hartmann
Physikalisches Institut der Universität Tübingen, Auf der Morgenstelle 14, D-72076 Tübingen, Germany
(Received 20 April 1998; revised manuscript received 19 August 1998)

The propagation of resonant 0π pulses in atomic rubidium is investigated experimentally and theoretically. In order to explain the observed pulse shaping, the hyperfine structure of the $D1$ transition for both isotopes is included. The influence of the hyperfine structure is also demonstrated by comparison between measurements in a natural mixture of atomic rubidium and pure rubidium 87. The characteristic difference between pulse shapes for moderate and large absorption is explained by means of a transfer function.
[S1050-2947(99)05901-6]

PACS number(s): 42.50.Gy, 42.65.−k, 42.50.−p

I. INTRODUCTION

The semiclassical theory for the propagation of resonant light pulses uses quantum-mechanical polarization together with Maxwell's equations [1]. Most attention has been paid to cases of strong resonant light pulses propagating through a two-level medium. Then many interesting effects, e.g., self-induced transparency, formation of solitons, and free-induction decay, occur [1–5]. In order to observe these effects, a sufficiently strong field, combined with a suitable duration of the pulse, is required. This leads to a significant change in the level occupation within a single pulse.

The subject of this work are weak pulses which leave the level occupation nearly unchanged. These 0π pulses change and exhibit a ringing in the tail of their pulse response. This was theoretically predicted in [6,7]. Further refinement of theory included laser chirp and Fresnel diffraction [8,9].

First experiments using 0π pulses in the ps time scale were made with atomic sodium and HCl [10,11]. The sodium experiment showed the expected ringing phenomenon with increasing ringing frequency for increasing absorption but no obvious effects caused by the hyperfine structure could be observed. In the HCl experiment, a beating signal due to the two isotopic species ^{35}Cl and ^{37}Cl could be seen but because of the fast decaying polarization the typical absorption-dependent ringing was not observable. More experimental work followed, investigating, e.g., the case of very high absorption [12] or the influence of 0π pulse propagation on four-wave mixing in solids [13].

We present measurements of 0π pulse shaping in atomic rubidium for two different regimes. For small absorption the pulse formation is dominated by the hyperfine structure, whereas for the case of strong absorption the typical ringing occurs, depending mainly on the total absorption. The following theoretical discussion therefore introduces a transfer function [14], which visualizes the influence of the hyperfine structure and the transition between small and strong absorption. The theoretical framework also allows for the introduction of a chirp in the light pulses, leading to a good agreement between measurements and simulations.

II. THEORY

The equation of motion for the nondiagonal density-matrix element ρ_{ab} of a two-level system with levels $|a\rangle$ and $|b\rangle$, submitted to a linearly polarized electric field $E(z,t)\hat{e}_x$ of the form

$$E(z,t)=\frac{1}{2}\mathcal{E}(z,t)e^{i(kz-\omega t)}+\text{c.c.}, \tag{1}$$

becomes in the rotating-wave approximation

$$\dot{\rho}_{ab}=-[i(\omega_0-\omega)+\gamma_{ab}]\rho_{ab}-i\frac{\mu}{2\hbar}\mathcal{E}\rho_d\,. \tag{2}$$

Here $\mu=-e\langle a|\hat{x}|b\rangle$ is the electric dipole moment, γ_{ab} the dipole dephasing rate, ω_0 the transition frequency, and ρ_d the difference in the population probability between the two levels. ρ_{ab} is given in the rotating frame of the electric field with frequency ω.

For small pulse areas Θ,

$$\Theta(z)=\int_{-\infty}^{+\infty}\frac{\mu}{\hbar}\mathcal{E}(z,t)\,dt, \tag{3}$$

it can be shown that the population difference ρ_d remains nearly constant [7]. If we assume the system initially to be in the ground state , this leads to the approximation $\rho_d(z,t)\approx -1$. Then Eq. (2) reduces to

$$\dot{\rho}_{ab}=-[i(\omega_0-\omega)+\gamma_{ab}]\rho_{ab}+i\frac{\mu}{2\hbar}\mathcal{E}, \tag{4}$$

which can easily be solved. With a Fourier transformation, which is symmetric with respect to ν and t, one obtains

$$\tilde{\rho}_{ab}(\nu)=i\frac{\mu}{2\hbar}\frac{\tilde{\mathcal{E}}(\nu)}{\gamma_{ab}+i(\omega_0-\omega-2\pi\nu)}. \tag{5}$$

Since we are interested in the polarization of an inhomogeneously broadened system with a distribution function $g(\omega_0)$ and the atomic number density N, we have to calculate the complex envelope $\mathcal{P}(z,t)$ of the polarization and $\tilde{\mathcal{P}}(z,\nu)$, respectively. Using an equivalent representation for the polarization as for the electric field in Eq. (1), $\tilde{\mathcal{P}}(z,\nu)$ is given by

$$\tilde{\mathcal{P}}(z,\nu)=N\int_{-\infty}^{+\infty}2\mu\tilde{\rho}_{ab}(z,\nu,\omega_0)g(\omega_0)\,d\omega_0. \qquad (6)$$

Equation (6) has been derived for a two-level system but can be generalized to situations in which more than two levels are involved. A small pulse area also decouples the nondiagonal elements of the density matrix in a multilevel system, since the coherence between substates, produced by a single pulse, is negligible [15]. Even in the case of coherent excitation with pulse trains of suitable repetition frequency, only a small amount of coherence between sublevels is attainable. We therefore treat the total polarization as a superposition of the polarization of many inhomogeneously broadened two-level systems. Then, assuming a set of Doppler-broadened transitions with transition frequencies ω_k, dipole moments μ_k, and weights g_k, one obtains for the polarization

$$\tilde{\mathcal{P}}(z,\nu)=-\frac{N}{\hbar}\tilde{\mathcal{E}}(z,\nu)\sum_k\frac{\mu_k^2 g_k}{i/T_2+[2\pi\nu+(\omega-\omega_k)]}. \qquad (7)$$

Despite a Gaussian distribution for Doppler broadening, we used a sum of Lorentzian line-shape functions for ease of analytical calculation. Here the total dephasing rate $1/T_2=\gamma_{ab}+1/T_2^*$ is given by the sum of the homogeneous dephasing rate γ_{ab} and the dephasing rate $1/T_2^*$ due to Doppler broadening.

Now we are in the position to apply Maxwell's equations in the slowly varying envelope approximation (SVEA). With the polarization of Eq. (7), the differential equation for the electric field is given by

$$\left(\frac{\partial}{\partial z}-i\frac{2\pi\nu}{c}+A(\nu)\right)\tilde{\mathcal{E}}(z,\nu)=0 \qquad (8)$$

with

$$A(\nu)=i\frac{\omega N}{2\epsilon c\hbar}\sum_k\frac{\mu_k^2 g_k}{i/T_2+[2\pi\nu+(\omega-\omega_k)]}. \qquad (9)$$

In Eq. (9), c and ϵ are the speed of light and the dielectric constant of the host medium, respectively, in which the polarizable atoms are embedded. The solution of Eq. (8) can be obtained directly and reads

$$\tilde{\mathcal{E}}(z,\nu)=\tilde{\mathcal{E}}(z=0,\nu)\exp\left(i\frac{2\pi\nu}{c}z-A(\nu)z\right). \qquad (10)$$

Since we are interested in a solution, given in the time domain, an inverse Fourier transformation has to be applied. With the retarded time $t'=t-z/c$, the electric field is the convolution of the electric field at $z=0$ and the inverse FT of the function $\exp(-A(\nu)z)$:

$$\mathcal{E}(z,t')=\mathcal{E}(z=0,t')\otimes\mathcal{FT}^{-1}(e^{-A(\nu)z}). \qquad (11)$$

Equation (11) suggests that the knowledge of the transfer function

$$T(\nu,z):=e^{-A(\nu)z}=|e^{-A(\nu)z}|e^{i\varphi(\nu,z)} \qquad (12)$$

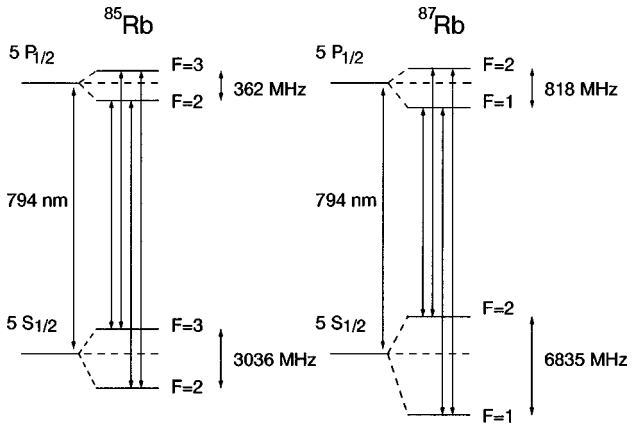

FIG. 1. $D1$ Transition with hyperfine structure for ^{85}Rb and ^{87}Rb.

is sufficient to calculate the modifications on 0π pulses propagating in a multilevel system [14].

III. MEASUREMENTS AND SIMULATIONS

Here we investigate the pulse propagation through atomic rubidium with the light of a mode-locked semiconductor laser tuned to the $D1$ transition of rubidium at 794 nm. Figure 1 shows the hyperfine structure of both isotopes. In addition, Fig. 2 displays the resulting $|T(\nu,z)|^2$ at small absorption for the natural isotopic mixture of rubidium (72% ^{85}Rb and 28% ^{87}Rb). According to Eqs. (10) and (12), $|T(\nu,z)|$ gives the absorption of the individual frequency components of the electric field, and therefore $|T(\nu,z)|^2$ in Fig. 2 resembles a typical absorption spectrum for rubidium. The two lines on the left and right margins of the spectrum represent the four transition frequencies for ^{87}Rb, while the four transition frequencies for ^{85}Rb cannot be resolved. Here each of the two stronger lines in the middle of the spectrum consists of two broadened transitions.

The initial light pulses exhibit a nearly Lorentzian shape and have a width (FWHM) of 15 ps; the spectral width of the pulses is about 100 GHz. The pulses are coupled into a cor-

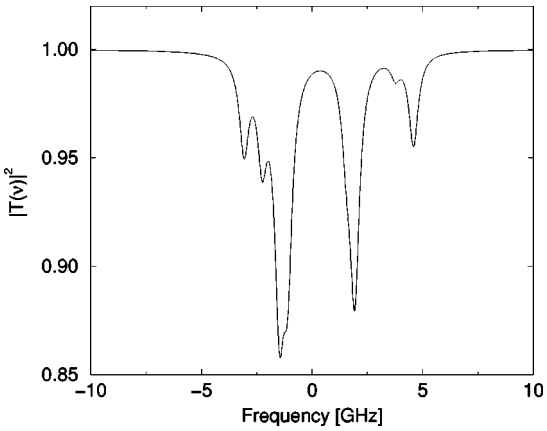

FIG. 2. Absorption spectrum of the $D1$ transition of rubidium in the natural isotopic mixture at small absorption.

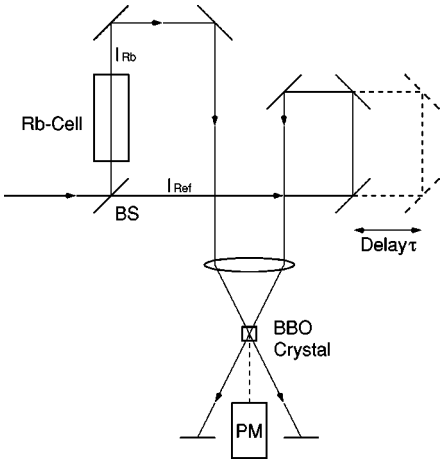

FIG. 3. Correlation setup. The beamsplitter (BS) divides the incident light pulses into reference and measurement pulses. For the reference pulses, delay times up to 800 ps are possible.

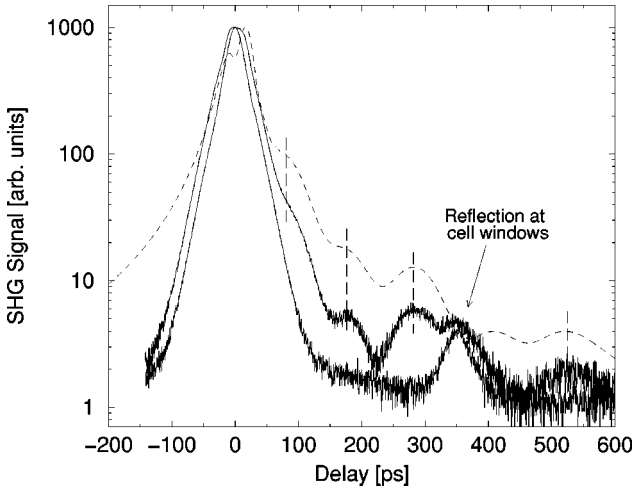

FIG. 4. Correlation measurements for $\alpha_0 l \approx 0.2$, $T = 294$ K (lower curve) and $\alpha_0 l \approx 24$, $T = 348$ K (middle curve). The upper curve shows the simulation for a rubidium temperature of $T = 351$ K and a laser chirp of -6.6 GHz/ps.

relation measurement setup (Fig. 3) with a repetition frequency of 525 MHz. The light is linearly polarized and the measured average power in both parts of the correlator is 500 μW.

The measurement pulse traverses a heated rubidium cell, which contains natural rubidium (cell 5 cm) and ^{87}Rb (cell 10 cm), respectively. The correlation between measurement and reference pulse is measured by second-harmonic generation (SHG) in a BBO crystal. In this setup the second-harmonic intensity $I_{\mathrm{SH}}(\tau)$,

$$I_{\mathrm{SH}}(\tau) \propto \int_{-\infty}^{+\infty} I_{\mathrm{ref}}(t) I_{\mathrm{Rb}}(t-\tau)\, dt, \tag{13}$$

is measured as a function of the delay time τ and depends on the intensities $I_{\mathrm{ref}}, I_{\mathrm{Rb}}$ of the two pulses. Then $I_{\mathrm{SH}}(\tau)$ as the cross correlation between $I_{\mathrm{ref}}(t)$ and $I_{\mathrm{Rb}}(t)$ allows us to determine changes in the shape of the measurement pulse $I_{\mathrm{Rb}}(t)$.

According to the weak pulse intensity, the detected second-harmonic power is very small and in order to improve the signal-to-noise ratio the displayed curves are the average of ten cross correlation traces.

For comparison of measurements and theory, we have calculated the transmitted pulse by Eq. (11). The k transitions refer to the possible transitions with linearly polarized light in the partly degenerated $D1$ system (Fig. 1). The weights g_k were used to account for the natural abundance of the two isotopes. In the following we characterize our measurements and calculations at small, moderate, and large absorption by the absorption $\alpha_0 l$. Following [11], the absorption coefficient α_0 is defined as the sum of the on-resonance absorption coefficients of the different $D1$ transition components for weak cw excitation. This procedure is appropriate since the frequency spectrum of the light pulses is much broader than the hyperfine structure of the $D1$ line.

A. Small and moderate absorption

Figure 4 shows measurements for small absorption at room temperature and moderate absorption together with the simulation for moderate absorption.

The measurement for small absorption is practically not influenced by the rubidium atoms, only a delayed pulse can be seen due to the reflection at the cell windows. For increasing temperature and atomic number density, respectively, the formation of weak delayed pulses is observed. In this regime the delayed pulses are not regularly ordered and the intensity is not monotonically decreasing. The simulated correlation in Fig. 4 shows the same behavior, using a slightly higher temperature ($\Delta T \approx 3$ K) for the simulation than measured. If the total absorption is varied in experiments or simulations, a change up to approximately 20% leads to qualitatively similar correlations with different spacings between the delayed pulses. Further change then produces correlations, which differ also in shape.

Part of the remaining difference between measurement and simulation (Fig. 4) in the signal height can be explained by the assumption of an initially Lorentzian light pulse, which produces higher correlation signals than the experimental pulses which are only approximately Lorentzian. Also the laser chirp, which is not exactly known, influences the signal height. This influence will be demonstrated in the next section.

B. Large absorption

Further increase of the absorption changes the shape of the observed correlations. As can be seen in Fig. 5 and Fig. 6, a ringing occurs and the ringing frequency increases with higher absorption. Even in this regime the simulations show good agreement with the measured correlations.

In addition, Fig. 6 demonstrates the influence of the assumed laser chirp on the simulations. A linear chirp for the electric field in Eq. (1) is introduced by the transformation

$$\mathcal{E}(z,t) \rightarrow \mathcal{E}_{\mathrm{chirp}}(z,t) = \mathcal{E}(z,t) e^{ibt^2}. \tag{14}$$

The parameter b can be adjusted for the desired chirp. For a transformation limited Lorentzian pulse with a width of 15 ps, a spectral width of 15 GHz, would be expected [16]. Since we measure a spectral width of 100 GHz, a linear chirp

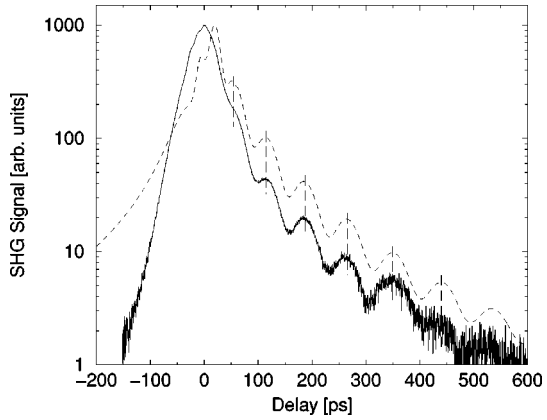

FIG. 5. Correlation measurement for $\alpha_0 l \approx 118$, $T = 371$ K (solid curve). The dashed curve shows the simulation for a rubidium temperature of $T = 372$ K and a laser chirp of -6.6 GHz/ps.

of -6.6 GHz/ps is used for the simulations. Figure 6 shows that the laser chirp strongly affects the resulting signal height but the separation of the following pulses does obviously not depend on the chirp.

C. Influence of the absorption spectrum

In the preceding sections a strong relation between total absorption and the resulting pulse shape could be seen. The influence of the absorption spectrum is observed for correlation measurements using only ^{87}Rb. Figure 7 shows the correlation measurement at an absorption of $\alpha_0 l \approx 24$. The simulated cross correlation in Fig. 7 resembles the measured correlation, whereas with the assumption of a natural isotopic mixture different results are produced. This is also experimentally confirmed since the correlation measurement in the natural isotopic mixture with similar absorption (Fig. 4) shows a qualitatively different structure. Furthermore, the correlation for the natural isotopic mixture indicates that the intervals between the delayed pulses are larger compared with the delayed pulses observed in pure ^{87}Rb. This behavior will be discussed in the next section.

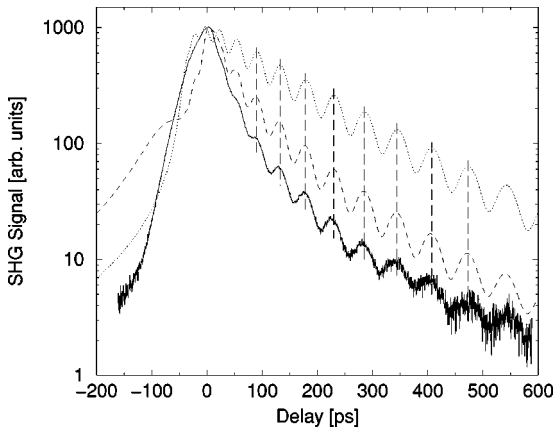

FIG. 6. Correlation measurement for $\alpha_0 l \approx 380$, $T = 390$ K (solid curve). The dashed curve shows the simulation for a laser chirp of -6.6 GHz/ps and a rubidium temperature of $T = 392$ K. The dotted curve shows the same simulation without chirp.

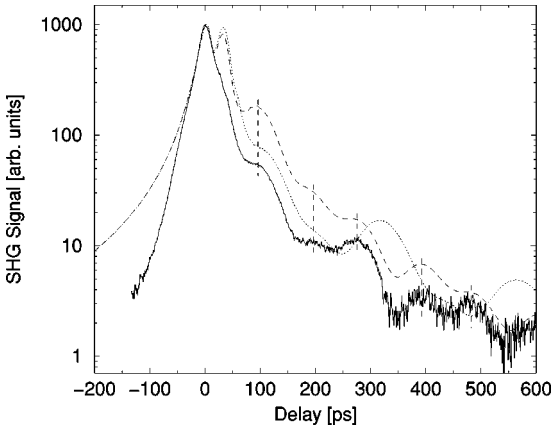

FIG. 7. Correlation measurement for $\alpha_0 l \approx 24$, $T = 339$ K (solid curve) in ^{87}Rb. The dashed curve shows the simulation for ^{87}Rb with a temperature of $T = 339$ K, the dotted curve shows the same simulation for the natural isotopic mixture.

IV. DISCUSSION

In order to examine the observed pulse shaping mechanism in both regimes, we consider the transfer function of Eq. (12). The absolute values of $T(\nu,z)$ indicate the absorption of the individual frequency components and $\varphi(\nu,z)$ describes the phase change. Since the frequency spectrum of the incoming pulse is much broader than the frequency range covered by the atomic transition, the shape of the transmitted pulse is mainly formed by the frequency components in the wings of the absorption line. For example, at the absorption $\alpha_0 l \approx 380$ of Fig. 9(b), the frequency components within ± 5 GHz on both sides of the absorption center are completely absorbed and do not contribute to the transmitted pulse.

To explain the occurrence of the delayed pulses, the polarization induced phase changes in the electric field have to be considered as the dominating mechanism. Then the superposition of all frequency components, including their phase changes, leads to the formation of the characteristic pulse shapes.

Figure 8 shows the interesting features of the transfer functions for moderate absorption, resulting in the correlation traces of Fig. 7. The absolute values more or less resemble the strongly broadened absorption spectrum of the $D1$ transition in rubidium. Phase changes close to π, indicated by deeper minima in the real part of $T(\nu)$, are located at the wings of the absorption lines. Therefore the appearance of the delayed pulses can be related to a beating of frequencies, which lie close to the transition frequencies. With this assumption the correlations in Fig. 7 can be interpreted. The arrows in Fig. 8(a) indicate the two outermost frequencies with phase reversal for the natural isotopic mixture. This frequency spacing appears to be smaller than for the ^{87}Rb case [Fig. 8(b)]. This larger frequency spacing is then found in the higher beating frequencies of the correlations (measured and simulated) for ^{87}Rb.

With increasing absorption almost the entire frequency range, spanned by the $D1$ transitions, is completely absorbed. This situation is depicted in Fig. 9. Figure 9(a) shows that even for frequencies with small absorption a large phase change occurs. Further increase of absorption then adds

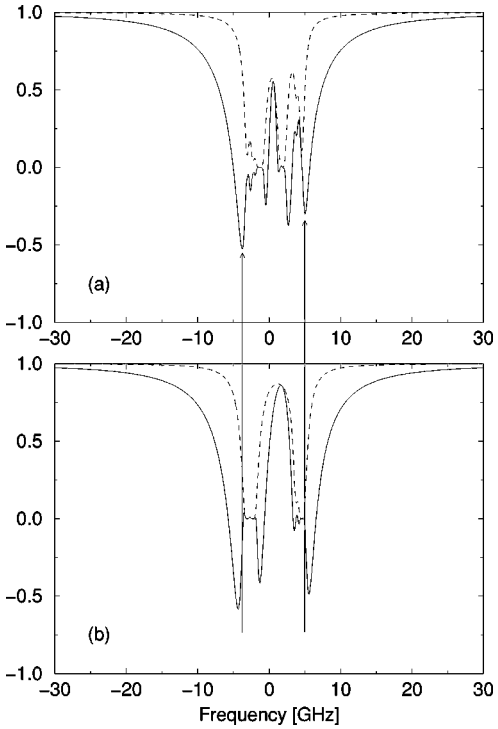

FIG. 8. Real parts (solid line) and absolute values (dashed line) of the transfer functions $T(\nu)$ used in the simulations of the measurement with $\alpha_0 l \approx 24$ (Fig. 7). (a) Transfer function for the natural isotopic mixture; (b) transfer function for ^{87}Rb.

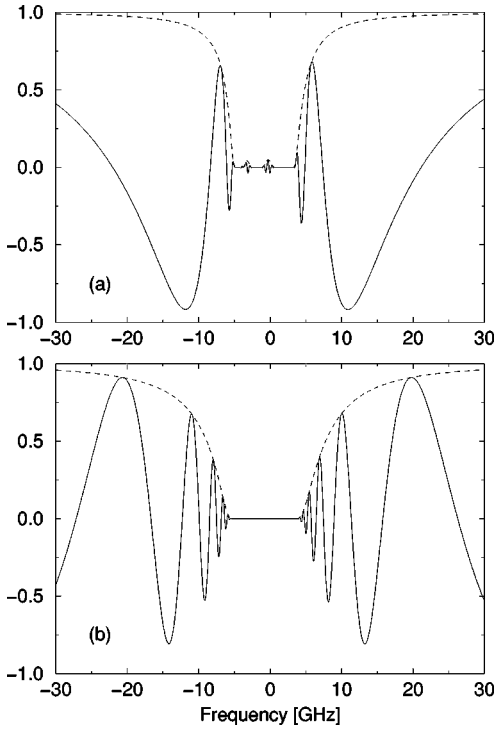

FIG. 9. Real part (solid line) and absolute value (dashed line) of the transfer function $T(\nu)$ used in the simulations of the measurements. (a) $\alpha_0 l \approx 118$; (b) $\alpha_0 l \approx 380$.

higher frequency components with reversed phase [Fig. 9(b)]. This leads to a higher ringing frequency, which can be observed in correlation traces for large absorption.

V. CONCLUSION

The theory of resonant 0π pulse propagation can be generalized to situations in which propagating pulses are resonant with more than two levels. The approximation of constant level occupation allows for the decoupling of the involved sublevels, leading to an analytical solution of the pulse propagating problem.

Experiments using the $D1$ transition of atomic rubidium can be simulated with quantitatively good agreement if a laser chirp is introduced. The observed pulse shaping exhibits a transition from a hyperfine structure dominated regime to a regime that shows the typical ringing in the tail of the pulse.

The transfer function of the investigated system imparts an understanding of the mechanisms for the pulse shaping. Here for the two regimes the influence of absorption and phase changes on the pulse shape can be studied in the frequency domain. This helps to explain the origin of the different shapes of the observed pulses and to predict pulse shaping in systems not investigated yet.

[1] L. Allen and J. Eberly, *Optical Resonance and Two-Level Atoms* (Wiley, New York, 1975).
[2] S. McCall and E. Hahn, Phys. Rev. **183**, 457 (1969).
[3] R. Slusher and H. Gibbs, Phys. Rev. A **5**, 1634 (1972).
[4] P. Meystre and M. Sargent III, *Elements of Quantum Optics* (Springer, Berlin, 1990).
[5] D. Mills, *Nonlinear Optics* (Springer, Berlin, 1991).
[6] D. Burnham and R. Chiao, Phys. Rev. **188**, 667 (1969).
[7] M. Crisp, Phys. Rev. A **1**, 1604 (1970).
[8] M. Crisp, Appl. Opt. **11**, 1124 (1972).
[9] S. Prasad and R. Glauber, Phys. Rev. A **31**, 1575 (1985).
[10] J. Rothenberg, D. Grischkowsky, and A. Balant, Phys. Rev. Lett. **53**, 552 (1984).
[11] H. Hartmann and A. Laubereau, J. Chem. Phys. **80**, 4663 (1984).
[12] M. Matusovsky, B. Vaynberg, and M. Rosenbluh, J. Opt. Soc. Am. B **13**, 1994 (1996).
[13] O. Kinrot and Y. Prior, Phys. Rev. A **51**, 4996 (1995).
[14] D. Champeney, *Fourier Transforms and their Physical Applications* (Academic Press, London, 1973).
[15] J. Mlynek, W. Lange, H. Harde, and H. Burggraf, Phys. Rev. A **24**, 1099 (1981).
[16] K. Sala, G. Kenney-Wallace, and G. Hall, IEEE J. Quantum Electron. **16**, 990 (1980).